# Experimental measurements of field effects on dielectronic recombination cross sections and Rydberg product-state distributions

A. Müller,* D. S. Belić,† B. D. DePaola,‡ N. Djurić,§ G. H. Dunn,**
D. W. Mueller,†† and C. Timmer
*Joint Institute for Laboratory Astrophysics, National Bureau of Standards and University of Colorado, Boulder, Colorado 80309-0440*
(Received 9 February 1987)

Experimental details are presented for the measurement of the effects of extrinsic electric fields on cross sections and Rydberg product-state distributions for dielectronic recombination of $Mg^+$ with electrons. A new type of Rydberg state detector is described. Experimental results for dielectronic recombination in the presence of fields are presented for three field values, and these results are compared with theoretical calculations.

## I. INTRODUCTION

We recently presented[1] results which unequivocally demonstrate experimentally that dielectronic recombination in the presence of electric fields (DRF) is both quantitatively and qualitatively different from dielectronic recombination in the absence of fields (DR). In this paper we present important experimental details which could not be treated in the brief format of a Physical Review letter. We also consider here the DRF mechanism and comparison of experimental and theoretical results in more detail.

The process of dielectronic recombination was apparently[2] first suggested as a recombination mechanism by Sayers in 1939 and first considered quantitatively by Massey and Bates[3] in 1942. It was not until 1964, however, when Burgess[4] showed its importance in resolving discrepancies in the ionization balance of the solar corona, that DR began to be considered on a regular basis as one of the key mechanisms in hot plasmas. Extensive theoretical work ensued, and the excellent review in 1976 by Seaton and Storey[2] summarizes the theory and the importance of DR in applications. Another review in 1980 by Dubau and Volonte[5] summarizes observations of DR satellite lines and details the importance of DR to applications in astronomy. Burgess and Summers[6] recognized early a peculiar feature of DR, that it could be dramatically affected by the mixing of angular momentum states, and they treated the effect of collisions in this context. Jacobs *et al.*[7,8] recognized that electric fields could mix $l$ states and strongly influence dielectronic recombination, and DRF was treated by them from the special perspective of the influence of plasma microfields. A later paper by Grigoriadi and Fisun[9] also treated this problem.

Since the review by Seaton and Storey,[2] a large number of other theoretical papers[10–33] have appeared besides the ones mentioned above. We cite only representative examples, but call particular attention to the paper by Bell and Seaton,[19] which develops the general theory of DR, and the papers[10–18] which deal with DRF, the topic of this paper. Some other papers cited have played roles in the exciting interplay between experiment and theory during the past four years. With the work of Burgess[4] came general recognition of the importance of DR in hot plasmas, but despite this it was not until 1978 that rate coefficients for DR were first measured by Brooks *et al.*[34] and by Breton *et al.*[35] by analyzing the time histories of ions in a $\theta$-pinch plasma and in a tokamak sawtooth discharge, respectively. Other work[36–39] of similar nature has followed. In the $\theta$-pinch papers particularly, the uncertain role of field and density effects has been emphasized. Careful spectroscopy on the DR satellite lines in highly ionized plasmas of tokamaks has yielded[40–45] DR rate coefficients for some highly ionized species under conditions where external fields should play no role. Another recent and successful method for studying the process for highly charged ions involves the collision of high-energy ions with gas targets and observing the process of resonant transfer and excitation (RTE).[46–50] Experimental methods and measurements for DR have been recently reviewed by Dunn.[51]

Experimental breakthroughs occurred about four years ago when several laboratories were able to directly observe DR and measure cross sections[52–56] under colliding beams conditions where the DR process could be definitely isolated. In all cases the measured cross section values were significantly larger than calculated ones. This led to additional theoretical activity,[29–33] but it was not until it was recognized[11] that fields play a role in the experiments, and that DRF is the process being observed, that progress was made towards harmonizing theory[11–18] and experiment. Particularly in the experiment[52] on $Mg^+$, the fields in the collision region were well defined, and the initial qualitative agreement between the experiment[52] and DRF estimates[11] prompted more detailed theoretical work[12–18] as well as the experiments reported here and earlier.[1]

Here we present unambiguous experimental evidence for the variation of DRF cross sections with electric field and show that the Rydberg state distribution of DRF products is also strongly field dependent. We describe the experimental techniques used, describe test measurements,

 

give an interpretation of the effects of angular-momentum state mixing, and compare measurements with theory.

## II. DIELECTRONIC RECOMBINATION—THE PROCESS

Dielectronic recombination can be thought of as the resonant radiationless capture of an electron by an ion to a doubly excited state of a once-less-charged ion, followed by radiative stabilization of that state. This can be represented by

$$e+X^{q+}\rightarrow(X^{(q-1)+})^{**}\rightarrow(X^{(q-1)+})^{*}+h\nu\ . \tag{1}$$

Thus, an electron is incident on an ion with an energy $\Delta E-\varepsilon$, i.e., just $\varepsilon$ less than the threshold energy $\Delta E$ needed to excite a bound electron of the ion. As the electron approaches the ion, it gains kinetic energy in the Coulomb field, so that in close it has more than enough kinetic energy to excite the bound electron. If it does so, however, the incoming electron no longer has enough energy to escape, and is bound in Rydberg level $n$ with binding energy $\varepsilon$. Since there is an infinite number of Rydberg levels, the DR capture cross section versus electron energy consists of a corresponding infinite series of resonances located just below the threshold for core-electron excitation. If the excited core electron radiates the excess energy away, dielectronic recombination results. If the energy of the excited core electron is again transferred to the Rydberg electron, autoionization occurs, the electron leaves, and the event appears as a resonance in the elastic scattering cross section.

In the description here, for simplicity's sake, we ignore radiative stabilization of the doubly excited complex by radiation from the high Rydberg state. In $Mg^{+}$ such transitions are not important;[13] however, in general, they must be taken into account, as has been emphasized by Gau and Hahn[57] and by Griffin and Pindzola.[58]

The fist step in this process can be described by a cross section $\sigma_c$ for electron capture. The fraction undergoing radiative stabilization of the intermediate doubly excited state is determined approximately by the branching ratio $[A_r/(A_r+A_a)]$, where $A_r$ and $A_a$ are transition rates for radiation and autoionization, respectively. The cross section for DR into a given state is then

$$\sigma=\sigma_c[A_r/(A_a+A_r)]\ . \tag{2}$$

The capture of a free electron into a doubly excited state is the inverse of autoionization. From the principle of detailed balance, it follows that $\sigma_c=kA_a$, where $k$ is a proportionality factor including the ratio of density of states. The DR cross section for capture into a state represented by quantum numbers $n,l$ can then be written as

$$\sigma_{n,l}=\sigma_0 2(2l+1)\left[\frac{A_a(n,l)A_r(n,l)}{A_a(n,l)+A_r(n,l)}\right], \tag{3}$$

where $\sigma_0$ involves various constants, includes a reciprocal dependence upon threshold energy $\Delta E$ and upon the energy width $\delta E$, and also involves the statistical weights of the initial state and of the core state of the product; $2(2l+1)$ is the statistical weight of the final Rydberg state $n,l$.

The high Rydberg electron is effectively a "spectator" as far as the radiation of the core excited electron is concerned, so that $A_r(n,l)$ is nearly constant with $n$ and $l$. On the other hand, $A_a(n,l)$ varies as $n^{-3}$. For "low" $n$'s and $l$'s $A_a \gg A_r$, where the inequality defines what we mean by 'low'; numbers may be $A_a\sim10^{14}\ s^{-1}$, $A_r\sim10^{8}\ s^{-1}$. Under these conditions $\sigma_{n,l}\propto A_r(n,l)$. At high enough $n$'s $A_a=A_r$, and beyond that $A_r>A_a$; so at high $n$, $\sigma_{n,l}\propto A_a(n,l)\propto n^{-3}$.

Similarly, $A_a(n,l)$ decreases rapidly with $l$ (see, e.g., Refs. 2 , 4, and 13), and $\exp(-\alpha l^2)$ with $\alpha=0.25$ may be chosen as a reasonable representative of this dependence. The total DR cross section is a sum over all the final resonance states covering the combinations of $n$ and $l$. For a given (low to moderate) $n$, and for low $l$, again, $A_a \gg A_r$ so $\sigma_{n,l}\propto(2l+1)\ A_r$; and for high $l$, $\sigma_{n,l}\propto(2l+1)e^{-\alpha l^2}A_r$. This is visualized with the aid of Fig. 1 which shows a hypothetical $A_a$ and $A_r$ versus $l$ for constant $n$ and also shows a result $\sigma_{n,l}$ (all solid curves). Thus, though the number of resonances which could contribute to DR increases as $\sum_{l=0}^{n-1}2(2l+1)=2n^2$, only $l$'s for $l\le l_c$ will typically contribute, where $l_c$ is the value of $l$ for $A_a(n,l)=A_r(n,l)$, and

$$\sigma_n=\sum_{l=0}^{n-1}\sigma_{n,l}\approx\sum_{l=0}^{l_c}\sigma_{n,l}=\sigma_0 2(l_c+1)^2A_r\ .$$

While this imposes no limitation for small $n$'s where $l_{\max}=n-1<l_c$, already for moderate $n$'s all possible contributions from $l$'s with $l_c\le l\le n-1$ are suppressed because of the strong decrease of $A_a$ with $l$. This becomes even more dramatic with high $n$'s where the $n^{-3}$ depen-

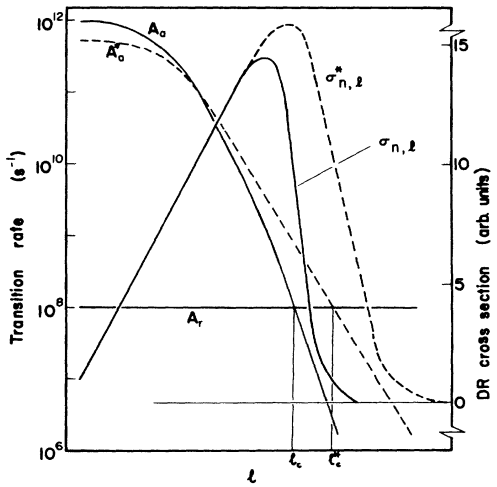


FIG. 1. Autoionizing rate $A_a$, radiative rate $A_r$ (both left ordinate scale), and the corresponding dielectronic recombination cross sections $\sigma_{n,l}$ (right ordinate) vs the azimuthal angular-momentum quantum number $l$ of the Rydberg state into which capture takes place. The solid curves are for no external fields, while the dashed curves ( * labels) are for a nonzero electric field mixing angular momenta according to the discussion in the text.

dence of $A_a$ leads to a strong decrease of $l_c$ and hence of the DR cross section. For $n=20$, where $2n^2=800$, $l_c$ may lie[13] between 5 and 10; if $l_c=10$, then the number of states contributing to DR is only about 200 out of the possible 800. There is thus a large "reservoir" of states which could contribute to DR if their autoionization rates were larger.

The role played by an electric field is to "tune" excluded states into the reaction by mixing the wave functions. With an electric field on, the autoionization rate becomes a weighted average of the rates $A_a(n,l')$ and is calculated by a relation similar to Eq. (5). As $E_c$ increases from zero, $l'$ states with $l' \neq l$ are mixed into the wave function and, in particular, states of high $l$ have components of lower $l'$ which have stronger coupling to the continuum; thus, the autoionization rate $A_a^*(n,l)$ for these mixed states is increased. [By the same reasoning, $A_a^*(n,l)$ is decreased for small $l$.] The value of $l_c$ (Fig. 1) is thus increased to $l_c^*$; i.e., more states effectively participate in the recombination process, and the cross section

$$\sigma_n^* \approx \sum_{l=0}^{l_c^*} \sigma^*(n,l)$$

is increased. The qualitative behavior just described for $A_a^*$ and $\sigma_c^*$ is illustrated by the dashed curves in Fig. 1.

In fact, of course, when an electric field is introduced in the collision region, the wave functions $\phi_{n,l,m}$ for $E_c=0$ have to be replaced by linear combinations of $\phi_{n,l',m}$ $[0 \leq l' \leq n-1]$, i.e., states of different $l$ (same $n$) are mixed in the field. (The following discussion is presented to give insights to the physical processes and is not intended as a theoretical description. Theoretical extensions of the Bell and Seaton[19] *ab initio* theory are given by Harmin[17] and by Sakimoto,[18] and these papers—as well as other DRF theory papers[8-16]—should be consulted for more rigorous statements of the theory.) The wave functions of Rydberg electrons are in the linear-Stark approximation[11,13]

$$\Psi^{\dagger}_{n,k,m} = \sum_{l=|m|}^{n-1} C_{n,k,m,l}\phi_{n,l,m} \ , \tag{4}$$

where $C_{n,k,m,l}$ are the Clebsch-Gordon coefficients related to the $3j$ symbol and $k=n_1-n_2$ is the electric quantum number. The parabolic quantum numbers $n_1$ and $n_2$ are determined from the equation $n=n_1+n_2+|m|+1$. The dagger in Eq. (4) and in the following designates quantities for $E_c>0$ in the linear-Stark approximation.

When exchange is neglected the autoionization rates $A_a(n,l)$ transform to

$$A_a^{\dagger}(n,k,m) = \sum_{l=|m|}^{n-1} |C_{n,k,m,l}|^2 A_a(n,l) \ , \tag{5}$$

while the radiative rates in the field $A_r(n,k,m)$ can be assumed to be equal to $A_r=A_r(n,l)$. With the changes in the autoionization rates the cross sections also change and become

$$\sigma_n^{\dagger} = \sigma_0 \sum_{m,k} 2\frac{A_a(n,k,m)A_r}{A_a(n,k,m)+A_r} \ . \tag{6}$$

This equation can be employed to estimate the maximum field enhancement of the DR cross section.

Figure 2 shows results of some simple model calculations employing Eq. (3) for the no-field case (solid curves) and Eqs. (5) and (6) when a field is present (dashed curves) and the states are mixed to a maximum extent. The model is for the case $\Delta n \neq 0$, where $A_r$ scales as $q^4$, where $q$ is the charge on the target ion, and $\Delta E$ scales as $q^2$. Thus, the starting points were $A_a(n,l) = 6\times10^{15}(1/n^3)\exp(-0.25l^2)$ s$^{-1}$, $A_r = q^4 3\times10^8$ s$^{-1}$, and $\sigma_0 = 3\times10^{-30}/q^2$. Results are shown for $q=1$, 4, and 20, demonstrating the successively smaller role of field mixing as $q$ increases; for $\Delta n=0$, the scaling is more complex. The radiative rate scales more slowly with $q$, and as $q$ increases the curves for $A_a$ versus $l$ become flatter,[13] so that $l_c$ may be larger. Nevertheless, a trend toward decreasing field dependence has also been predicted[13] as $q$ is increased for $\Delta n=0$ transitions.

In either case, for low and intermediate charge states, enhancement of DRF by large factors is seen. Clearly, the onset of this enhancement with $n$ will depend on field strength—stronger fields will be able to influence lower $n$ states. Thus, important experimental questions to answer about DRF revolve about the dependence on $n$ of the

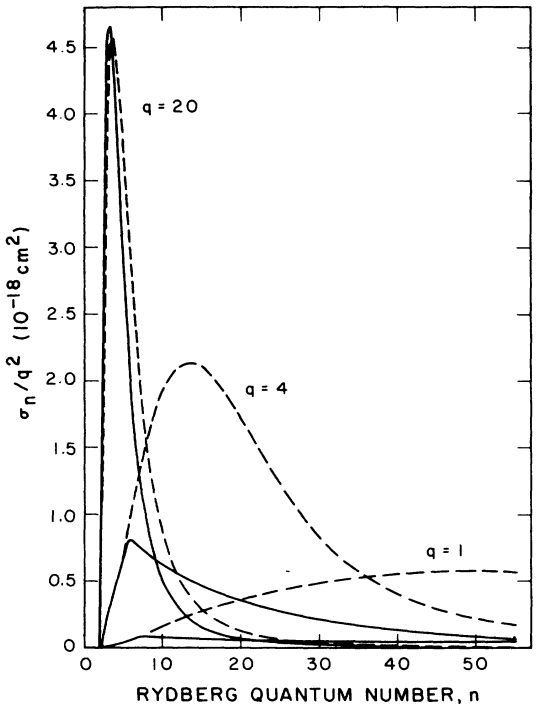


FIG. 2. Model cross sections $\sigma_n$ and $\sigma_n^{\dagger}$ vs Rydberg quantum number $n$ for ion charge states $q=1$, 4, and 20. For all calculations model transition rates $A_a$ and $A_r$ from Sec. II were used. The fat solid curves ($\sigma_n$) are obtained using Eq. (3) for the field free DR process. The dashed curves ($\sigma_n^{\dagger}$) are for results obtained from Eqs. (5) and (6) for maximum mixing in an electric field. For low $n$'s (same $q$) the cross sections $\sigma_n$ and $\sigma_n^{\dagger}$ do not differ from each other. The assumed interaction energy width is 0.5 eV for the model calculations.

DRF cross section for different fields in the collision region.

## III. EXPERIMENT

### A. General

In the experiments reported here we measured the cross section for

$$e+\mathrm{Mg}^+(3s)\leftrightarrow\mathrm{Mg}(3p,nl)\rightarrow\mathrm{Mg}(3s,nl)+h\nu \ . \tag{7}$$

The measurements were done such that cross sections versus electron energy were measured for fixed $n$, and cross sections versus $n$ were measured for fixed electron energy. These sets of measurements were made for different values of electric field in the collision region.

The crossed-beams technique was used as illustrated schematically in Fig. 3. A beam of mass-selected $^{24}\mathrm{Mg}^+$ ions with velocity $\mathbf{v}_i=\hat{\mathbf{i}}v$ is crossed by a magnetically confined, variable-energy beam of electrons traveling in the $y$ direction. In the ion-rest frame, the fields are $\mathbf{B}_c=\hat{\mathbf{j}}B$ and $\mathbf{E}_c=\hat{\mathbf{k}}vB$, and the electron-ion collisions occur in these fields. After collision, the ions and DRF product Rydberg atoms enter an electric field $\mathbf{E}_s=\hat{\mathbf{k}}E_s$ which deflects the $\mathrm{Mg}^+$ ions into a Faraday cup. The product atoms continue undeflected into a region with an electric field $\mathbf{E}_I(x)$ in the $x$-$y$ plane which varies along the atoms' flight path. This spatially varying field ionizes Rydberg atoms at different positions along the $x$ axis, depending on the quantum level, and the resultant electrons (or ions, depending on plate polarity) are detected using a position-sensitive detector. These electrons (or ions) are the "signal" of the experiment, representing (with relevant efficiencies accounted for) the number of atoms formed in "quantum level" $n_f$ as a result of DRF in collisions between the $\mathrm{Mg}^+$ ions and electrons.

The primary electron and ion beam currents $I_e$ and $I_i$ were measured, the number $N(n_f)$ of detected product Rydberg atoms from a given range $\Delta n_f$ of $n_f$'s were counted for a time $T$, the beams' spatial distributions $G(z)$ and $R(z)$ were measured, and the cross section $\sigma(n_f)$ for DRF was calculated from the relationship basic to colliding-beams[59] experiments,

$$\sigma(n_f)=\frac{[N(n_f)/T]e^2v_iv_eF}{I_eI_i(v_e^2+v_i^2)^{1/2}\epsilon\Delta n_f} \ . \tag{8}$$

Here $v_i$ and $v_e$ are the ion and electron velocities, and $\epsilon$ is the measured[60] detection efficiency of the position-sensitive detector for electrons (or ions). The form factor $F$ accounts for the spatial overlap of the two beams and is given by

$$F=\frac{\int R(z)dz\int G(z)dz}{\int R(z)G(z)dz} \ . \tag{9}$$

The "quantum number" $n_f$ is really a field index quantity given by

$$n_f=(3.2\times10^8/E_I)^{1/4} \ . \tag{10}$$

This is the principal quantum number of the hydrogenic eigenstate that just field ionizes in a field $E_I$ (V/cm) using a classical saddle-point model (see Appendix). Of course, the field-ionization lifetime depends on all the Stark quantum numbers, not just $n$. In the experiment there is only the field $E_I$ to distinguish states. The relationship of $n_f$ to "real" eigenstates is discussed in the Appendix.

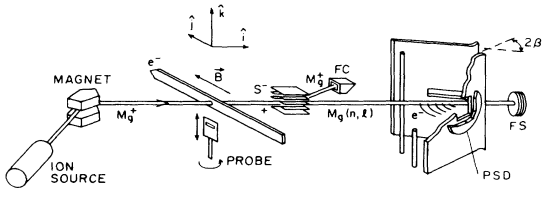


FIG. 3. Schematic of apparatus. In this figure the Rydberg-state analyzer detector is set to detect electrons.

### B. Electron and ion beams

The electron beam was produced in a gun patterned after the one developed by Taylor *et al.*,[61] the characteristics of which have been studied in detail. The entire gun is immersed in a magnetic field. The electron-ion interaction energy could be determined from

$$E_e=V_c-\phi-\frac{SI_e}{\sqrt{E_e}}+\frac{S_iI_i}{\sqrt{E_i}}+\Delta_F+\Delta_c \ . \tag{11}$$

Here $V_c$ is the applied potential difference between the gun cathode and interaction region, $\phi$ is the contact potential difference between these electrodes, $S=0.071$ $\mathrm{eV}^{3/2}\mu\mathrm{A}^{-1}$ and $S_i=3.0$ $\mathrm{eV}^{3/2}\mu\mathrm{A}^{-1}$ are geometric factors and the terms with these factors account for space-charge effects, $E_i$ is the ion energy, $\Delta_F$ is a possible energy shift due to penetration into the interaction region of electric fields from deflector plates located along the ion beam immediately before and after the electron gun, and $\Delta_c$ is the kinematic shift ($\approx m_e/m_iE_i$) of the electron-ion interaction energy. In practice the sum $(\Delta_F+\Delta_c-\phi)$ was determined experimentally by setting the Rydberg atom detector to detect $n_f=33$ states and monitoring the signal as the cathode potential was changed. The DRF resonance for capture into the state with $n_f=33$ occurs immediately ($\approx0.004$ eV) below the threshold for excitation at 4.43 eV. From the value of $V_c$ at the maximum signal (corresponding to $E_e=4.43$ eV) the value of $(\Delta_F+\Delta_c-\phi)$ could be calculated using Eq. (11).

Similarly, the width of the electron-energy distribution is given by

$$\Delta E_e=\Delta E_{\mathrm{th}}+S'I_e/\sqrt{E_e} \ , \tag{12}$$

where $\Delta E_{\mathrm{th}}\approx0.25$ eV is the thermal width due to the temperature of the cathode and the second term is a space-charge term with $S'=0.017$ $\mathrm{eV}^{3/2}\mu\mathrm{A}^{-1}$. However, in practice it is more accurate to again use the measured $\sigma$ $(n_f=33)$ versus $E_e$ curve to determine $\Delta E_e$. Since the true cross section is essentially a $\delta$ function, the observed cross-section shape is a direct measurement of the form of the energy distribution. In fact, both approaches give the same width to within 10%. Electron currents between 10

and 30 $\mu$A and an energy width $\Delta E_e \approx 0.5$ eV [full width at half maximum (FWHM)] were typical for the measurements reported here, and the beam was $2\times5$ mm$^2$ at the interaction region (Fig. 3). Electron densities were thus in the range $10^6$–$10^7$ cm$^{-3}$.

The $Mg^+$ ions were produced in a simple, commercial, hot-filament, discharge ion-source.[62] Strips of Mg metal were placed in the connecting feeder tube to the source, and the discharge was struck and sustained by Mg vapor (no added gases) at a discharge voltage of 40 V and current of 300 mA. The feeder tube had to be advanced periodically to keep an adequate supply of Mg in the vapor state. The ions were extracted, formed into a beam, mass analyzed by a sector field magnet, and transported via focusing and collimating optics to the interaction region where the beam was about 2 mm wide by 2–5 mm high. Ion currents were usually of order 300 nA, as measured by an electrometer attached to a Faraday cup into which the ions were deflected after the interaction region. The velocity of the ions was usually $1.27\times10^7$ cm s$^{-1}$ (2 keV energy).

For proper detection, it was important that the product neutral Mg beam reach a detector 70 cm downstream from the interaction region as a spatially thin and well-centered beam. Therefore, it was necessary that the ion beam at the collision region be well collimated and properly directed. The transverse (to the ions) magnetic field which collimates the electron beam and provides the mixing field $\mathbf{E}_c$ in the collision region deflects the ions beginning from a location well upstream. This had to be compensated for with the use of a series of deflectors, and with these and appropriate lenses, conditions were usually achieved so that the product neutrals at the detector were in the form of a beam 3–4 mm high and properly centered in front of the position-sensitive detector (PSD). Figure 4 shows a plot of the PSD signal integrated along the beam direction ($x$) versus the vertical direction ($z$). Notice that the signals fall well within the boundaries of the PSD and are centered on the device. Obtaining the correct focus and transport conditions necessary for this was often the most difficult part of setting up an experimental run. To assist in this process, both the PSD and a microchannel plate followed by a fluorescent screen located downstream from the ionizing plates were used as diagnostic tools.

Beam spatial distributions $G(z)$ and $R(z)$ used in Eq. (9) were measured by passing a 0.125-mm slit through a beam and recording the differential current passing through the slit at a given $z$. The probe was then rotated 90° and the procedure repeated for the other beam.

### C. Rydberg atom and state detector

The important problem of the detection and analysis of Rydberg atoms has been approached using a variety of techniques, but the method most commonly used involves field ionization.[63] Our need in these experiments was for a device which would detect continuous beams of particles with keV range energies and provide differential dispersion of the initial state. MacAdam and Rolfes[64] devised an elegant approach to solving this problem, employing an inhomogeneous electrostatic-field stripper followed by a conventional 127° cylindrical electrostatic energy analyzer and channel electron multiplier detector.

The method adopted here borrows from that of MacAdam and Rolfes[64] in using an inhomogeneous electric-field stripper. It differs, however, in that the stripper field also serves as the analyzer field, thus introducing some construction simplicity. The detector is a position-sensitive detector; this introduces additional versatility of resolution and diagnostic capability.

The device is shown schematically in Figs. 3 and 5. Two plates $15\times30$ cm$^2$ are mounted with a pivot along one long edge so the plates form a wedge with variable angle $2\beta$ between them. A voltage $\pm V$ is placed on the plates and a field

$$\mathbf{E}_I = V/(\beta R)\hat{\theta} \tag{13}$$

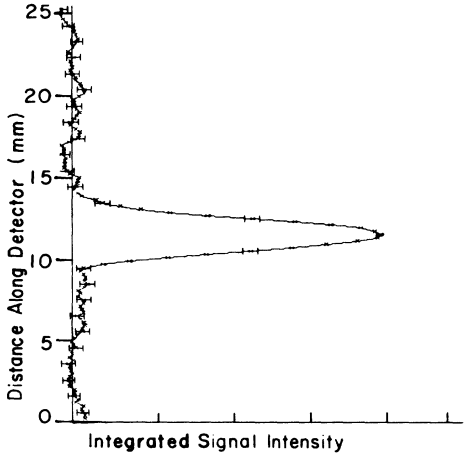


FIG. 4. Intensity of Rydberg-atom signal from DR along the vertical ($z$) coordinate of the PSD. The signal has been integrated in the horizontal direction.

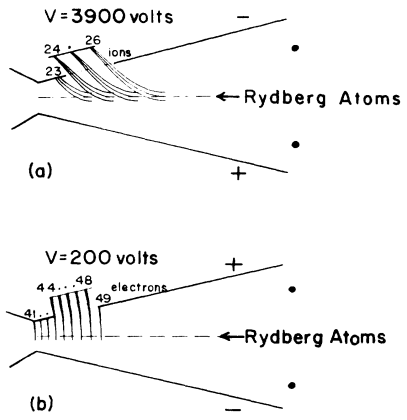


FIG. 5. Overhead schematic representation of Rydberg-state analyzer showing calculated trajectories for (a) ions and (b) electrons. The numbers in the detector regions indicate the calculated $n_f$ values.

results, where $R$ is the distance into the wedge from the apex. Wires are placed at 9° intervals at the open end of the wedge to minimize fringe field effects in the wedge. The other end of the plates has a 2-cm section bent out at 45° to soften fringe field effects at the apex end. Numerical field calculations with $\beta=15°$ show that fields in the critical region calculated with Eq. (13) differ at *most* by 0.1% with the numerically evaluated fields, and that difference occurs at the apex end of the detector "window" used. At the center of the detector window, the difference is only 0.02%. Since, by Eq. (10), $n_f$ depends on the $\frac{1}{4}$ power of $E_s$, differences in $n_f$ are totally negligible, so Eq. (13) is used throughout for all data analysis.

The detector window is a 2.86-cm square hole centered halfway up the plate and with one edge of the hole 1 cm from the bend at the apex end of the plate. On the inside of the plate, 25 wires of 0.075 mm diameter are spot welded along the $x$ direction; on the other side of the plate (1.5 mm thickness) a fine mesh grid (92.5% transparency, 1-mm hole size) is attached. Thus, voltages from subsequent parts of the detector cannot leak into the wedge region and alter particle trajectories. Behind the gridded detector window the position-sensitive detector[65] is located.

The PSD consists of two tandem 25-mm-diameter microchannel plates (MCP) mounted in a chevron configuration followed by a resistive anode. A grid mounted in front of the plates and biased 100-V negative with respect to the first MCP ensures a constant (and favorable) situation vis-a-vis collection of secondary electrons from the interchannel webbing of the MCP. The PSD electronics computes an $x$-$y$ coordinate for each pulse, and gives out a pair of digital numbers which are entered into a histogramming memory and eventually sent to a computer for processing.

Resolution is easily 0.25 mm, which compares with calculated separations using Eqs. (10) and (13) of several ($\sim 7$) millimeters for adjacent $n_f$ values. In a simple context one may thus expect to see separated "bumps" for the various $n_f$'s. However, there was generally not clear evidence for such separated bumps. The assumption is that there is a distribution of Stark states, so that such features would not be expected. The effect of the distribution of Stark states is discussed more in the Appendix.

The wedge plate opposite to that with the detector also has a rectangular hole in it, $2.8\times 12$ cm$^2$. Twenty-five wires of 0.075-mm diameter were attached equally spaced along this hole to keep the equipotential plane determined. Without this hole, when electrons (ions) are being detected, ions (electrons) from $n>n_f$ ($n<n_f$) could in principle hit the opposite plate and release secondary electrons or photons; this would give rise to possible "cross talk" of particles from states arriving at the opposite plate with those from states arriving at the detector. Tests showed that with the precautions taken, this cross talk was less than 1% of the potential amount (with honeycomb rather than "open space" behind the hole, cross talk up to 35% was found). The possible residual cross talk of the order 1% was ignored in the data reduction.

By choosing the polarity of voltages on the plates, one can observe either electrons or ions as the products of field ionization. The detection efficiency $\epsilon$ of the PSD for electrons and ions was determined[60] using beams of the relevant particle of about $10^{-15}$ A, measured with a vibrating-reed electrometer. The efficiencies are measured functions of impacting particle energy and are about $\epsilon\approx 0.7$. DRF cross-section values from detecting electrons or ions determined on the basis of these efficiency measurements are consistent and agree with each other to within 5%.

The range $\Delta n_f$ of detected Rydberg states was determined from trajectory calculations; some representative trajectories of both electrons and ions are shown in Fig. 5. It was possible to electronically change the detection range $\Delta n_f$ of the PSD; the detector window limits were $R_2^{\max}=6.96$ cm and $R_1^{\min}=4.46$ cm, where $R_1$ and $R_2$ are the distances of the detector's active edges from the apex of the wedge for $\beta=15°$, and the vertical limits were $z=\pm 1.25$ cm. For given $R_1$ and $R_2$ electronically set within those limits, $\Delta n_f$ for electron detection was calculated by assuming that a Rydberg atom in the "state" $n_f$ is field ionized when it reaches $E_I=3.2\times 10^8 n_f^{-4}$ V cm$^{-1}$, and the released electron follows the electric field lines to the detector. The range of $n_f$'s detected is determined by the edges of the detector

$$\Delta n_f = n_f(R_2)-n_f(R_1) \tag{14}$$

with

$$n_f(R_i)=\left[\frac{3.2\times 10^8 \beta R_i}{V}\right]^{1/4} . \tag{15}$$

The mean value of $n_f$ within the range $\Delta n_f$ is just taken as

$$n_f=\tfrac{1}{2}[n_f(R_2)+n_f(R_1)] . \tag{16}$$

These simple formulas give results which agree perfectly with results from full electron-trajectory calculations. For most measurements detecting electrons, $R_1=5.71$, $R_2=6.62$, giving $\Delta n_f=0.0369 n_f$. Ion trajectories are quite different from electron trajectories because of the initial momentum of the ions formed. The ions impact the detector at about 43° to the surface (compared to 90° for electrons) and $\Delta n_f$ for ions is smaller than $\Delta n_f$ for electrons for given $R_1$ and $R_2$. Trajectory calculations were relied upon totally for ions, since no simple formulas were found for ions analogous to Eqs. (14) and (16). Magnetic fields (dominated by the Earth's field) were canceled in the wedge volume to a level of about 5 $\mu$T. Without this cancellation, trajectories of electrons from high $n_f$ (low $E_I$) were materially affected by the magnetic field.

### D. Electric and magnetic fields

The primary purpose of this study was to determine the effects of fields in the interaction region on DR. It is, however, important to realize that fields in the beam path subsequent to the detector can affect the DRF product state distribution of Rydberg atoms. The importance of these fields and the fact that the fringe fields were estimated leads us to give here a fairly detailed description of the fields in the particles' paths.

As described in Ref. 61, the magnetic field $\mathbf{B}_c = \hat{\mathbf{j}}B$ which collimates the electrons and also gives rise to the collision-region electric field, $\mathbf{E}_c = \hat{\mathbf{k}}vB$, is from a magnet structure consisting of four 1.27-cm-diameter Alnico rod magnets centered on the corners of a 5.08-cm square and terminated by 8.89-cm-diameter Armco iron pole caps. To change the magnetic field, and thus change $E_c$, the entire electron-gun structure had to be disassembled and the Alnico rods replaced. Because of the difficulty of this change, only two values (0.02 and 0.006T) of magnetic field in the collision region were used.

It is clear that one can also change $E_c$ by changing the ion velocity $v$. However, the problem discussed in Sec. III c of "snaking" the ion beam through the transverse magnetic field and still ending with a well-defined and located neutral beam 70 cm downbeam is exacerbated with slow ions. Nevertheless, a small amount of data was obtained with 500 eV (instead of the "normal" 2000 eV) ions in the low (0.006 T) magnetic field.

The magnetic field continues for some distance past the $e$ gun, and bends the ions upward. However, an additional field is needed to bend the ion beam into a Faraday cup. This separation field is made by six plates 15 cm long stacked vertically 1.27 cm apart with linearly increasing negative potentials on them—thus giving a uniform field in the $z$ direction over the 15 cm length of the plates. They are shielded front and back with grounded plates. The front plate has a 3-cm square hole to allow entry of the ion and Rydberg atom beams, and the back has a 3-cm-wide by 7.6-cm-tall hole to allow passage of the undeflected Rydberg atoms and the strongly deflected ions which enter a Faraday cup.

After emerging from the separator plates, the Rydberg atoms pass through a tube 4.5-cm diameter and 13 cm long before entering the separate vacuum chamber containing the Rydberg-state analyzer-detector. The field (including the fringe field at the entrance) of this analyzer lies in the $x$-$y$ plane—thus the field is rotated by $\pi/2$ from the fields in the collision and separator regions. Since, as will be discussed more later, the changing fields may produce some changes in Stark-state populations, the fields along the beam path are plotted in Fig. 6. Solid and dashed curves show measured or otherwise well-known values; dotted curves are estimated fields based on knowledge of geometry and surfaces but too complex to calculate without unreasonable effort.

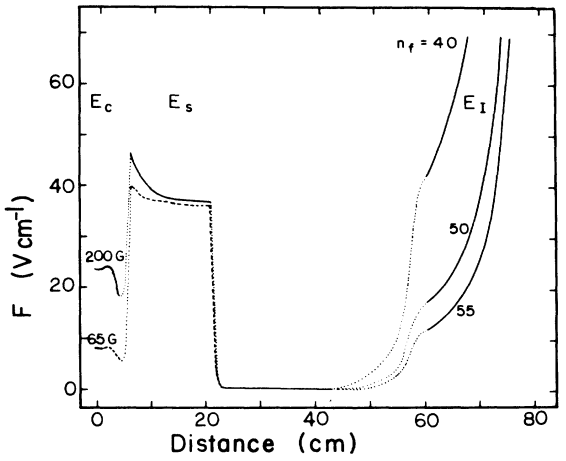


FIG. 6. Plot of electric field along the ion beam ($x$) axis, starting at the interaction region and proceeding through the Rydberg-state analyzer. The interaction field $E_c$ and separator field $E_s$ are in the $z$ direction, while the analyzing field $E_I$ is rotated by $\pi/2$ and lies in the $x$-$y$ plane. Fields in the analyzer region are shown only for three exemplary values of $n_f$ being detected. Solid and dashed lines indicate known field values; dotted lines are estimates.

### E. Data acquisition and other experimental features

As is often the case in electron-ion crossed-beams experiments the background counts at the detector far exceed the signal. Thus, collisions of the fast ion beam with background gas ($p \approx 1\times10^{-9}$ Torr$=1.3\times10^{-7}$ Pa) and with surfaces gave *average* (over $n_f$) background count rates of 750 s$^{-1}$. This compares with an average (over $n_f$) signal rate of 8.1 s$^{-1}$. To separate background from signal, the electron beam was gated on and off the DR resonance[56] at a 500-Hz rate. The "off-resonance" condition generally meant that the electron energy was shifted to a value about 2 eV higher than the DR resonance value. The gun-electrode potentials were modulated so that the electron current at the higher energy gave the same space-charge fields at the collision region—thus obviating any possible problems due to space charge changing of ion trajectories. Data from the "on" and "off" portions of the cycle were gated into two different histogramming memories, and the differences were taken between the two in the course of data reduction.

An experiment to measure cross section versus $n_f$ or cross section versus $E_e$ generally required many tens of hours integration. To insure that drifts in beam currents, particle trajectories, beam overlaps, etc., did not influence the data, the defining parameters were scanned in a time short compared to drift times. Thus, when measuring cross section versus $n_f$, the electron energy for a resonance was fixed at 4.43 eV and the voltages on the Rydberg analyzer plates were repeatedly scanned over 40 values corresponding to detection of integer separated values of $n_f$ [see Eqs. (15) and (16)] between 18 and 57. The single scan time was about 20 s with a dwell time of 322 ms at each voltage—a 72% duty cycle. When measuring cross section versus $E_e$, the voltages on the analyzer plate were fixed for $n_f = 33$, and the electron energy on resonance was scanned through a number (e.g., 27) of values separated by 0.1 or 0.05 eV. The scans were repeated several thousand times during a data run.

Thus, $\sigma(E_e)$ versus $n_f$ and $\sigma$ $(n_f)$ versus $E_e$ were obtained as relative data. Then $\sigma$ $(E_e = 4.43$ eV, $n_f = 33)$ was measured absolutely a number of times with all variables carefully controlled and measured. The scale could then be fixed for the scan sets described.

## IV. CORRECTIONS AND UNCERTAINTIES

The distance between the collision region and the detector is about 72 cm, giving a flight time of 5.7 $\mu$s for 2-keV

particles and 11.4 $\mu$s for 500-eV particles. During this time some of the Rydberg atoms may decay to other states by radiating photons. The lifetime of $p$ states is shortest and has been calculated[66] for hydrogen Rydberg atoms to be $T_{n,l=1} \simeq 2\times 10^{-10} n^3$ s. For $n=20$ this gives a lifetime of 1.6 $\mu$s, implying that 97% of the $20p$ state would not survive until the detector is reached. However, the statistical weight for the $p$ state is only $2(2l+1)=6$, while $n=20$ has a weight of $2n^2=800$. It is rather the average lifetime against radiative decay of a Rydberg atom with principal quantum number $n$ that has to be considered. Again, assuming a hydrogenic model should give a good estimate for Mg Rydberg atoms, the average lifetime is calculated[66] to be $\bar{T}_n = 6\times 10^{-11} n^{9/2}$ s. For $n=20$ the average lifetime is 42.9 $\mu$s, so possible losses are of order 10%. For $n=30$, $\bar{T}_n \simeq 266$ $\mu$s and the possible losses are of order 2%. Nevertheless, this discussion shows that an original Rydberg-state distribution formed by DR might be slightly changed due to atoms radiating before they reach the Rydberg-state detector. These changes are estimated to be negligibly small for $n \gtrsim 30$.

In addition to this small modification of the $n$-state distribution, it was pointed out by LaGattuta *et al.*[14] that there is a possibility that angular-momentum states are changed by the varying fields in transit to the detector. It has been shown by Rolfes *et al.*[67] and by Richards[68] that suddenly changing and rotating fields can drive Rydberg states toward high-$n_1$ Stark states corresponding to high angular momenta. The field $\mathbf{E}_I$ is rotated by $\pi/2$ from $\mathbf{E}_c$ and $\mathbf{E}_s$. As the particles enter the rotated analyzing field $\mathbf{E}_I$, they encounter a variable slew rate—which also depends on the $n_f$ being detected. As an example, for $n_f=40$ and 2-keV $Mg^+$ ions, the atom may encounter a slew rate up to $10^8$ V cm$^{-1}$ s$^{-1}$ in the fringe field. In the analyzer, the slew rate is given by $\rho_s = Vv/(\beta R^2) = 2.5\times 10^{16}/(n_f^4 R^2)$, and by the time the particle is opposite the center of the detector window ($R=6.17$ cm), this gives $\rho_s \sim 4.1\times 10^9$ V cm$^{-1}$ s$^{-1}$ for $n_f=20$, $\sim 2.6\times 10^8$ V cm$^{-1}$ s$^{-1}$ for $n_f=40$, and $1.0\times 10^8$ V cm$^{-1}$ s$^{-1}$ for $n_f=50$. Slew rates of the order of $4\times 10^8$ V cm$^{-1}$ s$^{-1}$ are also encountered in entering and leaving the separator field, but the field in this case is always in the $z$ direction. The rotation and slew rates encountered are such that one may, indeed, get a redistribution of $n_1$ states. Though this does not change the $n$ states, it does change the measured $n_f$ distribution, since field ionization probability depends on the Stark quantum numbers—not just $n$. This is discussed more in Sec. VI and in the Appendix.

Various possible corrections to the data will occur to the reader, and some of these—which were dealt with—are catalogued here. The first is a universal issue in counting experiments—dead time. The maximum (with $n_f$) average total (from the entire detector surface) count rate was about 2100 s$^{-1}$, and taken with the 8-$\mu$s dead time of the counting system, a correction of about 1.8% is implied. Implied corrections at other $n_f$'s ranged down to 0.9%, so that distortion of the distribution by ignoring dead-time corrections is a maximum 0.9%—dead time was ignored. Another effect arises from the fact that the Rydberg atom beam has a finite width. Hence, electrons or ions originating from field ionization of these atoms start from a range of equipotentials and thus have a range of energies when they strike the collector. Since the detector efficiency[60] is energy dependent, corrections to the data are implied. Using our measured efficiency curves, a correction $(1+2950 n_f^{-4})^{-1}$ was derived for multiplying the measured cross sections. Another correction $(1-4199 n_f^{-4})^{-1}$ was necessary on the basis of the pulse input level to the PSD electronics. The product of these leaves a net multiplicative correction of $(1+1249 n_f^{-4})$.

The PSD is preceded by several grids with some transmission. During the efficiency measurements it was found that slow electrons which are post accelerated to the PSD are focused through the grid holes and do not "see" one of these grids. For our situation, this implies that cross sections for $n_f \leq 24$ are corrected by 1/0.925, whereas cross sections for higher $n_f$'s are not corrected.

Uncertainties in the absolute value of cross sections measured here center primarily around uncertainties in measuring the quantities in Eq. (8) and in the statistical uncertainty of the data. In estimating systematic uncertainties, maximum possible levels have been taken, and the statistical uncertainty has been taken at 2 times the standard deviation, i.e., approximately 90% confidence level. The values and their quadrature sum, taken as the total uncertainty at "good confidence level" are presented in Table I.

## V. EXPERIMENTAL RESULTS

The results of these measurements have—for the most part—been presented earlier,[1] as noted at the beginning. However, for continuity and completeness they are presented here again. The weighted average of 13 measurements of $\sigma$ ($E_e=4.43$ eV, $n_f=33$) at $E_c=23.5$

Table I. Uncertainties in the absolute measurement of $\sigma$ ($E_c=4.43$ eV, $n_f=33$) and other relevant quantities. Statistical uncertainty is at the $2\sigma$ confidence level (90% CL) and total uncertainty is thought to be at a "good confidence" level, roughly equivalent to 90% CL.

| Source | Uncertainty (%) |
|---|---|
| $I_e$ | 2 |
| $I_i$ | 2 |
| $v_i$ | 0.5 |
| $\Delta n_f$ | 5 |
| $\epsilon$ | 5 |
| $F$ | 3 |
| Cross talk | 1 |
| Quad. sum–total systematic | 8 |
| Statistical ($2\sigma$) | 6 |
| Quad. sum | 10 |
| Total uncertainty in $\sigma(n_f)$ | |
| $\Delta E_e$ | 4 |
| $\bar{n}_f$ | 2 |
| Total uncertainty in $\Delta E\sigma$ | 11 |

$V\,cm^{-1}$ is $(7.12\pm0.24)\times10^{-19}$ $cm^2$; for 11 measurements at $E_c=7.2$ $V\,cm^{-1}$ the value is $(4.61\pm0.12)\times10^{-19}$ $cm^2$. Since DR and DRF cross sections are extremely narrow in energy, these numbers mean little without knowledge of the electron-energy distribution. Figure 7 shows $\sigma(n_f=33)$ versus $E_e$ for both $E_c=23.5$ and 7.2 $V\,cm^{-1}$. We define the strength $S(n_f)$ of the collision by

$$S(n_f)=\int\sigma(n_f,E_e)dE_e=\sigma(n_f,4.43)\Delta E_e\ . \qquad (17)$$

Using this, we have for $E_c=23.5$ $V\,cm^{-1}$, $S(33)=3.70\times10^{-19}$ $cm^2\,eV$ and $\Delta E_e=0.52$ eV; for $E_c=7.2$ $V\,cm^{-1}$, $S(33)=2.23\times10^{-19}$ $cm^2$, and $\Delta E_e=0.48$ eV. The difference in energy widths for the two cases is due to difference in electron current and hence differences in the space-charge term in Eq. (12). The total uncertainties in $S(33)$ are about 11% as shown in Table I.

Figure 8 shows $S(n_f)$ versus $n_f$ with the values of $S(33)$ determined by the absolute measurements above. With the instrumentation available, it was not possible to include a measurement for $n_f=17$ in the scans. Thus, the value of $S(17)$ for $E_c=23.5$ $V\,cm^{-1}$ was determined by two separate absolute measurements. The two points (solid triangles) for $E_c=3.6$ $V\,cm^{-1}$ (ion energy of 500 eV) were measured with a two point "sweep," and the point for $S(33)$ was measured absolutely separately. The uncertainty on the $n_f=18$ point in this case was larger than the value for both of two runs. The points at $n_f=33$ are separately absolute, and the outer error bars indicate total uncertainty, while the inner ones indicate statistical uncertainty. Bars on the other points are statistical only. For contrast the figure also shows the "no-field" prediction of Burgess[69] mapped, as discussed below, to the index $n_f$.

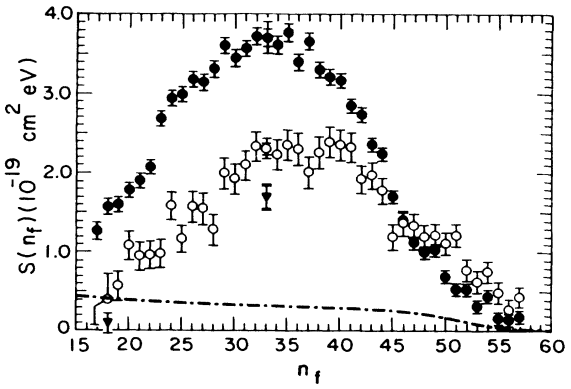


FIG. 8. Collision strength [Eq. (17)] $S$ vs $n_f$ with electron energy fixed at 4.43 eV. Filled circles, $E_c=23.5$ V/cm; open circles, $E_c=7.2$ V/cm; inverted triangles, $E_c=3.6$ V/cm. Dot-dashed curve is predicted (Ref. 69) value for $E_c=0$ V/cm. Uncertainties are one statistical standard deviation. For $n_f=33$ the total relative uncertainties are also shown. See Table I.

## VI. DISCUSSION AND COMPARISON WITH OTHER WORK

From Fig. 8 it is clear that at the fields used there is a strong dependence of $S(n_f)$ on $E_c$ for low and intermediate $n_f$'s. Past $n_f\approx45$ there seems to be no significant field influence. Thus, the cross-section magnitude is strongly affected by $E_c$, and the state distribution is severely altered. One could take a cut at any $n_f$ and plot $S(n_f)$ versus $E_c$. This is done at $n_f=33$, and the results are presented in Fig. 9. In the figure the value of $S(33)$ or $\sigma(33)$ at a given field value is divided by the value at $E_c=23.5$ $V\,cm^{-1}$. This makes it easier to compare *shapes* of variation with $E_c$, and in the figure there are also theoretical values of LaGattuta *et al.*[14] and Bottcher *et al.*[16] The curve is drawn between the more numerous theoretical points of LaGattuta *et al.* to guide the eye. Both theories and the experiment have points at or near 23.5 $V\,cm^{-1}$, and they are all normalized as noted above. The figure nicely demonstrates the strong "tunability" of the cross section with $E_c$ for $2\lesssim E_c\lesssim20$ $V\,cm^{-1}$, and the relative insensitivity outside that range. At the level at which comparisons can be made, there is reasonable

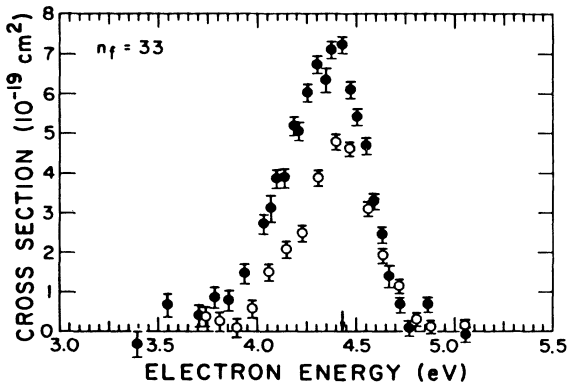


FIG. 7. Measured cross sections vs electron energy for DRF ($n_f=33$) in $Mg^+$ for two values of electric fields in the collision region: filled circles, $E_c=23.5$ V/cm; open circles, $E_c=7.2$ V/cm. Uncertainties are one statistical standard deviation.

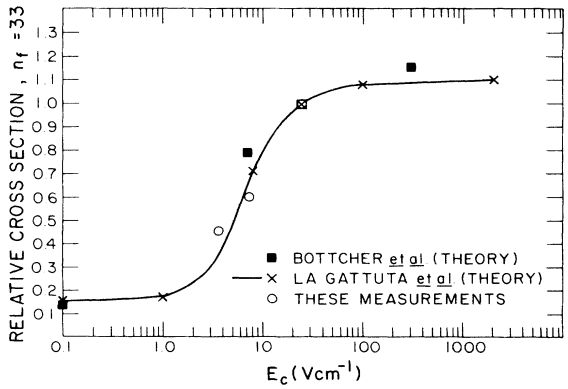


FIG. 9. Relative DRF cross sections for $Mg^+$ at $n_f=33$ vs field strength in the collision region. Open circles are present measurements; $x$'s, Ref. 14 and private communication, Y. Hahn; squares, Ref. 16. Measurements and theoretical values are normalized at $E_c=23.5$ V/cm. Solid curve connecting $x$'s is drawn to guide the eye.

agreement among the theoretical and experimental shapes. At $E_c = 23.5$ V cm$^{-1}$, there is almost full $l$ mixing.

If one forms the sum

$$S = \sum_{n_f} S(n_f) \tag{18}$$

over all values of $n_f$ for which $S(n_f)$ is significant, then $S$ corresponds to the total cross section integrated over energy. Table II lists values $S^{a}$ of total collision strength measured in this experiment. An extrapolation was performed to get $S(n_f)$ for $n_f < 17$, and this added 6% and 9% to the value of $S$ for $E_c = 23.5$ and 7.2 V cm$^{-1}$, respectively.

In an earlier experiment we measured[52] the total cross section using essentially the same apparatus as here with $E_c = 23.5$ V cm$^{-1}$, except that instead of the Rydberg analyzer there was a simple multiplier detector. For that measurement, the stabilizing photon from DRF [see Eq. (7)] was detected in coincidence with the Rydberg product. All quantities were measured absolutely *except* the detection efficiency of the multiplier for Rydberg atoms. This had to be estimated, and it was done as follows. The efficiency of the multiplier was measured for $Mg^+$ ions, and a value of 0.28 was found. It was then reasoned that there would be substantial field ionization between the grid at the entrance to the multiplier and the first dynode, and that therefore the sensitivity to the Rydberg atom would be higher than for ions. The value 0.65 was chosen—halfway between the ion value and 1.0, and an uncertainty $\pm 0.35$ was attached, acknowledging that the sensitivity could be anywhere between the ion value and 1.0. If one accepts the cross section arrived at in this way, and multiplies by the width (0.3 eV) of the electron beam in that experiment, one obtains $S = 3.3 \times 10^{-18}$ cm$^2$ eV for the total strength. If one argues that a Rydberg atom looks like an ion accompanied by a *slow* electron, then the sensitivity to Rydberg atoms should be much the same as for ions. Then, there results from that experiment[52] $S = 7.7 \times 10^{-18}$ cm$^2$ eV. These values are listed in Table II as $S^{b}$ and $S^{c}$.

The theoretical values of LaGattuta *et al.*[14] and Bottcher *et al.*[16] are also listed as $S^{d}$ and $S^{e}$, respectively. The agreement (except for the "uncorrected" previous measurement) is good, and the agreement for the $E_c = 7.2$ V cm$^{-1}$ case is especially striking.

TABLE II. Total collision strengths [Eq. (18)] for the two values of $E_c$: 23.5 and 7.2 V cm$^{-1}$. Units are $10^{-18}$cm$^2$ eV.

| $E_c$ (V cm$^{-1}$) | 23.5 | 7.2 |
|---|---|---|
| $S^{a}$ | 9.5 | 6.2 |
| $S^{b}$ | 3.3 | |
| $S^{c}$ | 7.7 | |
| $S^{d}$ | 7.4 | 6.3 |
| $S^{e}$ | 7.6 | 6.2 |

[a]Present value.
[b]From Ref. 52.
[c]"Corrected" from Ref. 52 (see text).
[d]From Ref. 14 updated by private communication, 1986.
[e]From Ref. 16.

The comparison of the detailed Rydberg-state distributions of Fig. 8 with theoretical calculations[14,16] requires a "mapping" of the theoretical distribution in Stark states with quantum numbers $n_1, n_2, m, n$ to the field ionization index number $n_f$. The physics necessary for such a mapping has been worked out by others for hydrogenic atoms, and this has been summarized and applied in the Appendix to the wedge field Rydberg-state analyzer developed for this experiment. Similar mappings were also done by LaGattuta *et al.*[14] and by Bottcher *et al.*[16]

With the material developed in the Appendix, we can proceed with the mapping needed for comparison. Figure 10 forms the focus of the discussion, where $S(n_f)$ is plotted versus $n_f$. The points are the same as those in Fig. 8 for $E_c = 23.5$ V cm$^{-1}$, and here the error bars represent the total absolute uncertainty. In order to get a "virgin" theoretical prediction in this same figure, we let the abscissa label have a double meaning—for the heavy solid curve (only) the abscissa numbering is for the principal quantum number $n$. The curve is the theoretical prediction of Bottcher *et al.*[16] *without* taking into account $3p_{3/2}nl \rightarrow 3p_{1/2} + e$ autoionization ($\frac{3}{2} \rightarrow \frac{1}{2}$ AI).

The separator field $E_s$ eliminates high Rydberg states from the theoretical $n$ distribution. The survival rates $P(n)$ from Fig. 14 in the Appendix can be used to calculate the Rydberg-state distribution arriving at the wedge-field detector under the assumption that there is no redistribution of states by the "collision with electric fields." (See the discussion of slew rates in Sec. IV.) The light

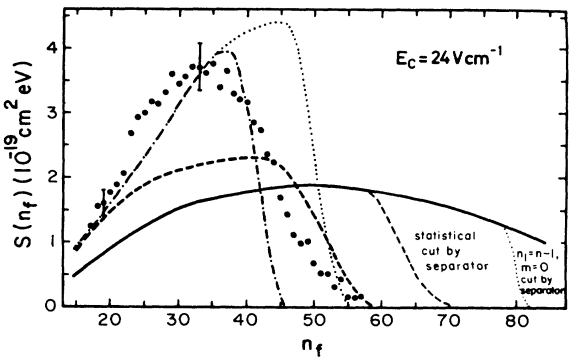


FIG. 10. Plot showing the effect of different mappings of theoretical DRF collision strengths to the $n_f$ coordinate. For the solid curve, the abscissa label is for $n$, the principal quantum number of the Rydberg state. For all other points and curves, the abscissa is $n_f$ as per Eq. (10). Points are same as Fig. 8 for $E_c = 23.5$ V/cm. Solid curve is theory (Ref. 16), no $\frac{3}{2} \rightarrow \frac{1}{2}$ AI case; effect of $E_s$ assuming statistical population of Stark Rydberg states, light dashed curve; effect of $E_s$ assuming energetically highest-lying Stark Rydberg state only, light dotted curve. The bold dashed curve represents the theory (solid curve, light dotted curve) assuming statistical populations of Stark states mapped to the coordinate $n_f$ [Eq. (10)]; bold dotted curve, theory (solid curve, light dotted curve) assuming only highest-lying Stark state populated mapped to $n_f$; dot-dashed curve mapped theory resulting from assuming statistical population entering the separator, but only highest Stark state entering Rydberg analyzer.

dashed curve in Fig. 10 joining the solid curve at about $n=58$ represents $P(n)S(n)$ assuming a completely statistical population of Stark states; the dotted curve joining the solid curve at about $n=78$ results when population of the energetically highest-lying Stark state only is assumed. Neither of the "cut" theoretical $n$ distributions is close to the experimental data shown versus $n_f$.

From the discussion earlier, we know that $n \neq n_f$ for a hydrogenlike system. If we assume a hydrogenlike situation for the Mg atoms investigated in this experiment, we can calculate detection probabilities $D(n,F)$ for our Rydberg-state analyzer [see Eq. (A8)]. We can then map the theoretical $S^{\text{th}}(n)$ so it can be compared to the experimental $S(n_f)$ using the relationship

$$S^{\text{th}}(n_f)=\frac{1}{\Delta n_f}\sum_n D(n,F)P(n,F)S^{\text{th}}(n)\ , \tag{19}$$

where $D(n,F)$ and $P(n,F)$ depend on the electric field and therefore can be expressed in terms of $n$ and $n_f$ as $D(n,n_f)$, $P(n,n_f)$ by using Eq. (10). The heavy dashed line in Fig. 10 represents a mapped $S^{\text{th}}(n_f)$ assuming a statistical population of all Stark levels in all phases of the experiment. Now theory and experiment are in much better agreement; however, theory is still considerably lower than experiment. Further investigation shows that this discrepancy may be attributable to the special assumptions made for the population of Stark levels. If we assume that within each $n$ manifold only the energetically highest Stark state with the longest field-ionization lifetime is populated, then we obtain the heavy dotted curve for $S^{\text{th}}(n_f)$ which increases even beyond the experimental values. We also calculated $S^{\text{th}}(n_f)$ under the assumption that a Mg atom beam enters the separator with a statistical Stark-state population, and then the population changes to $(n_1=n-1,\ m=0)$ only when it enters the rotated wedge field. The resulting dot-dashed curve for $S^{\text{th}}(n_f)$ is close to the experimental data and reproduces the maximum of the experimental $n_f$ distribution quite well. This exercise shows the ambiguity in the interpretation of the experimental data as long as assumptions have to be made about the Stark-level population in the Mg$(3s,nl)$ atomic beam after dielectronic recombination. The task for theory is the calculation of field-time effects for nonhydrogenic species. At the moment, however, a solution to this problem seems somewhere in the future.

Additional comparisons of $S^{\text{th}}(n_f)$ with the experiment are shown in Figs. 11 and 12 for the $E_c=23.5$ and 7.2 V cm$^{-1}$ cases, respectively. Solid error bars represent $1\sigma$ statistical uncertainties. The dashed bar at $n_f=33$ represents the 11% total uncertainty from Table I. In Fig. 11 the dashed curve is from Bottcher *et al.*[16] for no $\frac{3}{2}\rightarrow\frac{1}{2}$ AI. It is similar to the heavy dashed curve in Fig. 10 except for small differences resulting from using different separation fields in the mapping exercise and the fact that the population distribution of Stark states entering the analyzer was assumed[13,16] to be concentrated in the states with $m=0$–5. The solid curve is also from Bottcher *et al.* and includes $\frac{3}{2}\rightarrow\frac{1}{2}$ AI. The dot-dashed curve is from LaGattuta *et al.*[14] and includes $\frac{3}{2}\rightarrow\frac{1}{2}$ AI—thus it can be compared directly with the solid curve from

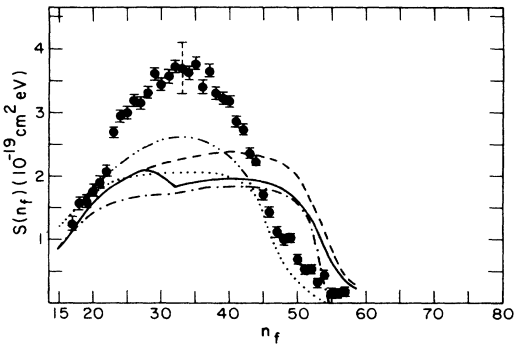


FIG. 11. Comparison of mapped theoretical $Mg^+$ DRF collision strengths vs $n_f$ with measurements (points) at $E_c=23.5$ V/cm. Dashed curve, Bottcher *et al.* (Ref. 16) no $\frac{3}{2}\rightarrow\frac{1}{2}$ AI accounted; solid curve, Ref. 16 with $\frac{3}{2}\rightarrow\frac{1}{2}$ AI; dot-dashed, LaGattuta *et al.* (Ref. 14) with $\frac{3}{2}\rightarrow\frac{1}{2}$ AI. Dotted and double-dot-dash, Ref. 14, with and without $\frac{3}{2}\rightarrow\frac{1}{2}$ AI, mapped assuming $n_2=0$.

Ref. 16. The dotted and double-dot-dashed curve are also from LaGattuta *et al.* and are for the cases with and without $\frac{3}{2}\rightarrow\frac{1}{2}$ AI and mapped with the assumption on the Rydberg-state distribution that $n_2=0$. The experimental curve is narrower and taller than any of these theoretical curves.

The discussion in the previous paragraph indicates that the possibility of state redistribution[67,68] in the fields between formation and detection may explain this difference seen in Figs. 10 and 11. But, if it were simply a matter of state redistribution, one would expect a similar difference between theory and experiment for $E_c=7.2$ V cm$^{-1}$. However, Fig. 12 shows that experiment and theory are seemingly in much better agreement for $E_c=7.2$ V cm$^{-1}$. (This was seen for the total $S$ also in Table II.) In the

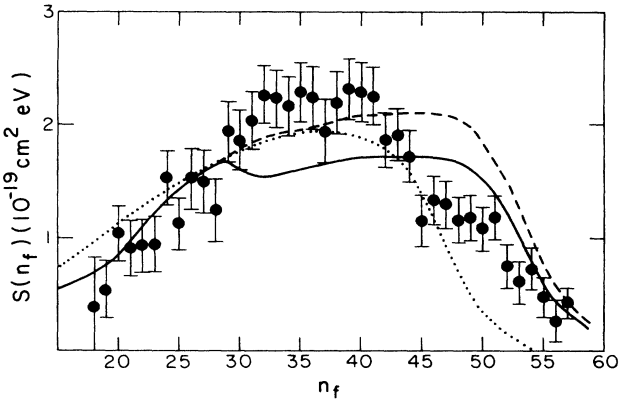


FIG. 12. Comparison of mapped theoretical $Mg^+$ DRF collision strengths vs $n_f$ with measurements (points) at $E_c=7.2$ V/cm. Curve notation same as in Fig. 11.

figure, the solid and dashed curves are the same as for Fig. 12, being from Ref. 16 and representing results with and wouthout $\frac{3}{2}\rightarrow\frac{1}{2}$ AI, respectively. The dotted curve is from LaGattuta *et al.*,[14] includes $\frac{3}{2}\rightarrow\frac{1}{2}$ AI, and is deduced with the assumption $n_2=0$.

One is led by the data and comparisons in Figs. 11 and 12 to the conclusion that significantly different Stark-state distributions result from DRF in the 23.5-V cm$^{-1}$ field than in the 7.2-V cm$^{-1}$ field. Since the same analyzing fields and associated slew rates and rotation rates are used for the data of both Figs. 11 and 12, it seems clear that the difference does not lie here. The electric and magnetic fields are different by approximately a factor of 3, and this must lead to decidedly different initial Stark-state distributions. It was seen in the discussion of Fig. 10 that this can make large differences in the shape of mapped curves.

It seems that the next important step in comparison of theory and experiment is to go back to the detailed theoretical information[13,16] on Stark-state populations at formation and follow them through the field-time histories to detection.

## VII. CONCLUSION

The data and discussion presented here and earlier constitute incontrovertible experimental evidence that electric fields in the collision region can tune the DRF cross section to a variety of values. The fields can also substantially alter the distribution of populations in the product Rydberg atoms. Instead of an order of magnitude difference between experiment and theory as was encountered three years ago, the differences are now in the range 15–25 % in the total cross sections. However, detailed comparisons of Rydberg-state distributions indicate that some issues remain unresolved. This and the fact that disagreements between experiment and theory persist in the experiments on DRF by Dittner *et al.*[56,70] and by Kohl *et al.*[71] indicates that more work should be done on DRF. It is clear that the new theoretical formulation of DRF by Harmin[17] and Sakimoto[18] should be applied to specific systems where experiments have been performed. The $Mg^+$ system for which results were presented in this paper is a good candidate for such calculations.

## ACKNOWLEDGMENTS

The authors thank C. Bottcher, D. Griffin, M. Pindzola, K. LaGattuta, and Y. Hahn for correspondence and data relative to their theoretical calculations. This work was supported in part by the Office of Fusion Energy of the U.S. Department of Energy under Contract No. DEAI01-76 PR06010 with the National Bureau of Standards. We also acknowledge the Hochschulrechenzentrum der Justus-Liebig-Universität Giessen for generously providing computer time and facilities. A. Müller acknowledges financial support of the Joint Institute for Laboratory Astrophysics Visiting Fellow Program and Max Kade Foundation. Work by D. Belić was partly made possible by the U.S.–Yugoslav Joint Board for Scientific Collaboration, Contract No. NBS(G)-279 YU.

## APPENDIX: ON THE IDENTIFICATION OF RYDBERG STATES BY FIELD IONIZATION

When a hydrogenlike ion (atomic number $Z$) in a Rydberg state $n$ with an energy $E_n=-Z^2/(2n^2)$ is exposed to an electric field of strength $F$, the Rydberg electron, in a classical picture not considering the Stark effect, can just escape when the saddle-point value $U(r_s)$ of the resulting potential $U(r)=-Z/r-Fr$ corresponds to the energy $E_n$. The saddle-point potential $U(r_s)$ is characterized by $\partial U(r_s)/\partial r=0$, from which results $r_s=\sqrt{Z/F}$ and $U(r_s)=-2\sqrt{ZF}$. Hence,

$$n=\left[\frac{Z^3}{16F}\right]^{1/4}, \tag{A1}$$

where $F$ is in atomic units ($5.142\times10^9$ V cm$^{-1}$). With unit conversion, we have Eq. (10), which was used to relate the electric field in the present experiment to a classical field-ionization quantum number called $n_f$.

In a real atom the presence of an electric field leads to Stark splitting and each Stark state with quantum numbers $n_1,n_2,m$, and $n=n_1+n_2+|m|+1$ has its own field-ionization lifetime $\tau(n_1,n_2,m,n)$ which depends on the field strength $F$. This lifetime can be calculated for hydrogenlike particles. Under the assumption of a statistical population of all Stark levels within one $n$ manifold at a given field strength $F$, the average survival probability $P(n,F)$ results

$$P(n,F)=\frac{1}{2n^2}\sum_{n_1,m}\exp[-\Delta t/\tau(n_1,n_2m,n,F)], \tag{A2}$$

where the assumption of a uniform distribution of Stark states leads to the statistical weight of each Stark state, $1/(2n^2)$. The summation extends over the quantum numbers $n_1$ and $m$ with $-(n-1)\le m\le(n-1)$ and $0\le n_1\le n-1-|m|$; $n_2$ is given by $n_2=n-1-|m|-n_1$. The dwell time $\Delta t$ is usually set within the range $10^{-6}$–$10^{-9}$ s. Similar to the classical field-ionization limit, Eq. (A1) [or Eq. (10)], one can find a relation between the "lowest" Rydberg quantum number $n$ that leads to field ionization and the field strength $F$. Such a relation is often quoted[72] to be

$$n=(6.2\times10^8\ \text{V cm}^{-1}/F)^{1/4}; \tag{A3}$$

however, it is not completely clear what assumptions were made in the derivation of this formula.

We have calculated $P(n,F)$ for electric fields between 17.9 and 6321 V cm$^{-1}$ corresponding to classical field-ionization limits at $n_f=65$ and 15, respectively. The lifetime $\tau(n_1,n_2,m,n,F)$ was inferred from a semiempirical formula for the field-ionization probability of hydrogen atoms developed by Damburg and Kolosov,[73]

$$\Gamma=\frac{1}{\tau}=\frac{(4R)^{2n_2+|m|+1}}{n^3n_2!(n_2+|m|)!}\exp[-\tfrac{2}{3}R-\tfrac{1}{4}n^3F(34n_2^2+34n_2|m|+46n_2+7m^2+23|m|+\tfrac{53}{3})]4.1341\times10^{16}\ \text{s}^{-1}. \tag{A4}$$

Here $R=(-2E_0)^{3/2}/F$ with $E_0$ the Stark energy in atomic units (27.2 eV) and $F$ also in atomic units. The Stark energy is calculated by means of a perturbation expansion up to $F^4$, which was given by Alliluyev and Malkin,[74]

$$E_0=-\frac{z^2}{2n^2}+\frac{3}{2}F\frac{n}{z}(n_1-n_2)-\frac{1}{16}F^2\left[\frac{n}{z}\right]^4[17n^2-3(n_1-n_2)^2-9m^2+19]$$
$$+\frac{3}{32}F^3\left[\frac{n}{z}\right]^7(n_1-n_2)[23n^2-(n_1-n_2)^2+11m^2+39]$$
$$+F^4\frac{n^{10}}{1024}[-5487n^4-147(n_1-n_2)^4+549m^4-1806n^2(n_1-n_2)^2+3402n^2m^2+1134m^2(n_1-n_2)^2$$
$$-35\,182n^2-5754(n_1-n_2)^2+8622m^2-16\,211]\ . \tag{A5}$$

Results obtained with these formulas are in very good agreement with exact calculations[73] for $n=7$ and also for higher $n$ values.[75] For a dwell time $\Delta t=10^{-6}$ s our results for $P(n,F)$ are shown versus $n$ in Fig. 13 with $n_f$ as a parameter that characterizes the field strength $F$. The quantum numbers $n$ for which $P(n,F)=0.5$ can be related to the corresponding values of $n_f$, the ratio $n(0.5)/n_f$ being between 1.19 for $n_f=15$ and 1.25 for $n_f=65$. The average in the present range of $n_f$ values is $n(0.5)/n_f=1.23$. Hence the field-ionization limit can be expressed as

$$n=(3.2\times10^8\ \mathrm{V\,cm^{-1}}\times1.23^4/F)^{1/4}$$
$$=(7.3\times10^8\ \mathrm{V\,cm^{-1}}/F)^{1/4}\ . \tag{A6}$$

From the ratio calculated for $n_f=15$ we would just obtain Eq. (A3). This is the result of the fact that even for a statistical average over all Stark levels an equation of the form $n=(\xi/F)^{1/4}$ with a constant $\xi$ is not exactly applicable, since $\xi$ depends slightly on $n$. However, the difference in the calculated ionization limits resulting from Eqs. (A3) and (A6) is only 3%.

Variation of the dwell time $\Delta t$ between $10^{-6}$ and $10^{-9}$ s leads to an increasing calculated value for $\xi$ with $\xi=7.81\times10^8$ V cm$^{-1}$ for $\Delta t=10^{-9}$ s. Again, the actual ionization limit $n$ changes very little in this range: $n(0.5)$ is only about 1.6% above the result expected from Eq. (A6). For the longest- and shortest-lived Stark states only, i.e., $(n_1=n-1,\ m=0)$ and $(n_1=0,\ m=0)$, the $\xi$ values obtained in the present range of fields are $\xi=16.2\times10^8$ V cm$^{-1}$ and $\xi=4.7\times10^8$ V cm$^{-1}$, respectively, indicating the uncertainty of a field-ionization method to identify Rydberg states in an unknown ensemble of atoms. Thus, the total range of $n$ values, which can be found at a given field strength $F$, is between $0.89n$ ($\xi_0$) and $1.22n$ ($\xi_0$) where $\xi_0=7.3\times10^8$ V cm$^{-1}$ [see Eq. (A6)].

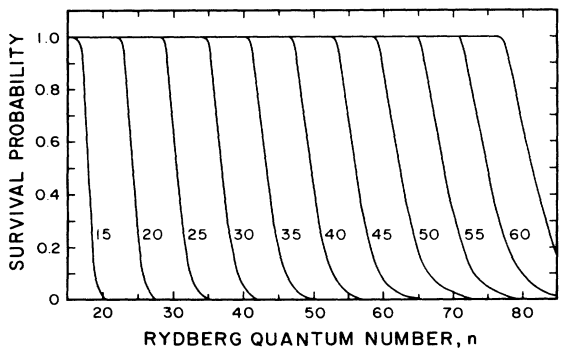


FIG. 13. Average survival probability of hydrogenic Rydberg atoms with principal quantum number $n$ exposed to an electric field for $10^{-6}$ s. Field strength, characterized by $n_f$ [Eq. (10)], parametrizes the different curves. Statistical population of Stark levels in each $n$ manifold is assumed.

In our experiment we apply a voltage to the separator plates (labeled $S$ in Fig. 3) corresponding to a field of 37 V cm$^{-1}$. If a certain distribution in the population of Stark states is assumed one can calculate survival probabilities for each Rydberg quantum number $n$ in this field. For a statistical population of Stark states one obtains

$$P(n)=\frac{1}{2n^2}\sum_{n_1,m}\exp\left[-\int_{x=0}^{L}\frac{dx}{v\tau(F)}\right]\ . \tag{A7}$$

The length $L$ of the separator is 15 cm, the velocity of our 2-keV Mg atoms is $v=1.27\times10^7$ cm s$^{-1}$. From Eq. (A4) the different values of $\tau(F)$ can be calculated. The resulting $P(n)$ is shown in Fig. 14 (dashed curve) versus Rydberg quantum number $n$. Equation (A7) is also especially applicable to a spatial distribution of electric field strength. The real field strength in the separator differs from 37 V cm$^{-1}$ by the $\mathbf{v}\times\mathbf{B}$ contribution of the magnetic fringing field downstream of the electron gun (see Fig. 6). When this contribution is taken into account the bold solid curve in Fig. 14 results for the survival probability $P(n)$. The extreme cases for $P(n)$, again using the real field distribution from Fig. 6, are shown by the thin solid lines in Fig. 14 for Stark states with $(n_1=n-1,\ m=0)$ and $(n_1=0,\ m=0)$ only. As expected from the above considerations, the values for $n(0.5)$ in these extreme cases differ from each other by about 30%, which represents the maximum uncertainty of the cutoff in the Rydberg-state distribution by the separator field.

With the wedge field subsequent to the separator, we try to identify the distribution of the Rydberg states surviving the separator field $E_s$. Again assuming a statistical population of Stark levels, we can calculate the detection probability $D(n,F)$ for each Rydberg quantum number $n$,

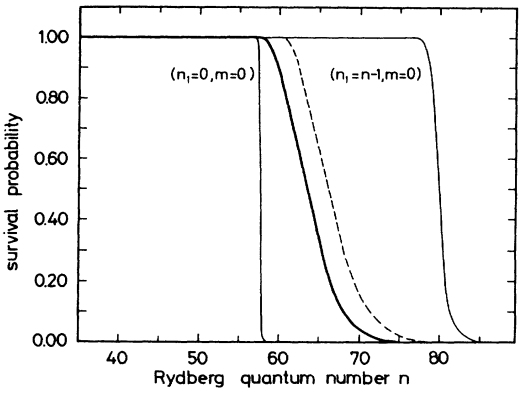


FIG. 14. Survival probability in a hydrogenic approximation of 2-keV Rydberg Mg atoms passing the separator field $E_s$ (15 cm length). Dashed curve, statistical population, assumed constant 37-V/cm field; bold solid curve, statistical population, actual (Fig. 6) $E_s$; thin solid lines, different assumptions on Stark-state populations shown on figure, actual $E_s$.

$$D(n,F)=\frac{1}{2n^2}\sum_{n_1,m}\left[\exp\left[-\int_{R_{\max}}^{R_2}\frac{dx}{v\tau(x)}\right]-\exp\left[-\int_{R_{\max}}^{R_1}\frac{dx}{v\tau(x)}\right]\right]. \quad \text{(A8)}$$

The field-ionization lifetime $\tau$ [see Eq. (A4)] depends on $x$ via the field strength $E_I(x)=V/[\beta R(x)]$, $R_1$ and $R_2$ are the edge positions of the effective detector area, and $R_{\max}$ is the distance between the apex of the wedge and the cylindrical surface containing the wires in front of the wedge field. The detection probability $D(n)$ for the given geometry was calculated for 2-keV Mg atoms. The electric fields in the center of the effective detector window

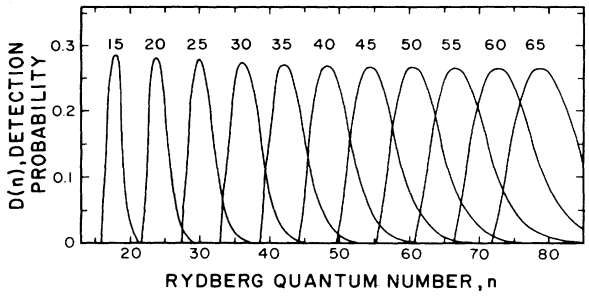


FIG. 15. Detection probability for Mg Rydberg atoms of the Rydberg state wedge field detector vs principal quantum number $n$. The parameter $n_f$ on each curve is related to the voltage on the detector plates through Eq. (15).

were varied between 17.9 and 7321 V cm$^{-1}$ corresponding to $n_f=65$ and 15, respectively. The integrations in Eq. (A8) were performed in 1-mm or 0.5-mm steps and were started 4 or 14 mm before the detector window. In all variations the same results were obtained, indicating that the approximation was convergent for the conditions applied. The resulting detectabilities $D(n)$ are shown in Fig. 15 versus Rydberg quantum numbers $n$, with $n_f$ as a parameter, which, by Eq. (10), corresponds to a given voltage $V$ applied to the plates of the wedge. The $n$ values belonging to the maxima in the distributions $D(n)$ for a given field strength in the center of the effective detector window are in good agreement with the values expected from Eq. (A6). The detector width $\Delta n$ can be calculated for a given field strength and classical field-ionization quantum number $n_f$, respectively. It turns out that $\Delta n$ is a linear function of $n_f$ with $\Delta n=0.0455n_f$. In the simple classical picture the corresponding relation was $\Delta n_f=0.0369n_f$ with a proportionality factor which is smaller by $(7.3/3.2)^{1/4}$ [see Eqs. (A1) and (A6)].

*Present address: Institut für Kernphysik, Strahlenzentrum der Justus-Liebig-Universität, Giessen, D-6300 Giessen, West Germany.
†Present address: Department of Physics and Metrology, Post Office Box 550, University of Beograd, Beograd, Yugoslavia.
‡Present address: Institute of Physics, Post Office Box 57, 11001 Beograd, Yugoslavia.
§Present address: Department of Physics, Kansas State University, Manhattan, KS 66506.
**Quantum Physics Division, National Bureau of Standards, Boulder, CO 80309-0440.
††Present address: Department of Physics and Astronomy, Louisiana State University, Baton Rouge, LA 70803-4001.

[1]A. Müller, D. S. Belić, B. D. DePaola, N. Djurić, G. H. Dunn, D. W. Mueller, and C. Timmer, Phys. Rev. Lett. **56**, 127 (1986).
[2]M. J. Seaton and P. J. Storey, in *Atomic Processes and Applications,* edited by P. G. Burke and B. L. Moiseiwitsch (North-Holland, Amsterdam, 1976), p. 134.
[3]H. S. W. Massey and D. R. Bates, Rep. Prog. Phys. **9**, 62 (1942).
[4]A. Burgess, Astrophys. J. **139**, 776 (1964); Ann. Astrophys. **28**, 774 (1965).
[5]J. Dubau and S. Volonte, Rep. Prog. Phys. **43**, 199 (1980).
[6]A. Burgess and H. P. Summers, Astrophys. J. **157**, 1007 (1969).
[7]V. L. Jacobs, J. Davis, and P. C. Kepple, Phys. Rev. Lett. **37**, 1390 (1976).
[8]V. L. Jacobs and J. Davis, Phys. Rev. A **19**, 776 (1979).
[9]A. K. Grigoriadi and O. I. Fisun, Fiz. Plasmy **8**, 776 (1981) [Sov. J. Plasma Phys. **8**, 440 (1982)].
[10]W. A. Huber and C. Bottcher, J. Phys. B **13**, L399 (1980).
[11]K. LaGattuta and Y. Hahn, Phys. Rev. Lett. **51**, 558 (1983).
[12]A. P. Hickman, J. Phys. B **17**, L101 (1984).
[13]D. C. Griffin, M. S. Pindzola, and C. Bottcher, Oak Ridge National Laboratory Report No. ORNL/TM-9478, 1985 (unpublished).
[14]K. LaGattuta, I. Nasser, and Y. Hahn, Phys. Rev. A **33**, 2782 (1986).
[15]D. C. Griffin, M. S. Pindzola, and C. Bottcher, Phys. Rev. A **33**, 3124 (1986).

[16]C. Bottcher, D. C. Griffin, and M. S. Pindzola, Phys. Rev. A **34**, 860 (1986).
[17]D. Harmin, Phys. Rev. Lett. **57**, 1570 (1986).
[18]K. Sakimoto, J. Phys. B **18**, 3011 (1986); **20**, 807 (1987).
[19]R. H. Bell and M. J. Seaton, J. Phys. B **18**, 1589 (1985).
[20]A. L. Merts, R. D. Cowan, and N. H. Magee, Jr., Los Alamos Scientific Laboratory Report No. LA 6220-MS, 1976 (unpublished).
[21]R. D. Cowan, *The Theory of Atomic Structure and Spectra* (University of California Press, Berkeley, 1981), p. 549.
[22]T. Fujimoto, T. Kato, and Y. Nakamura, Nagoya Institute of Plasma Physics, Report No. IPPJ-Am-23, 1982 (unpublished).
[23]L. J. Roszman, in *Physics of Electronic and Atomic Collisions,* edited by S. Datz (North-Holland, Amsterdam, 1982), p. 641.
[24]K. LaGattuta and Y. Hahn, J. Phys. B **15**, 2101 (1982).
[25]K. LaGattuta and Y. Hahn, Phys. Rev. Lett. **50**, 668 (1983).
[26]D. J. McLaughlin and Y. Hahn, Phys. Rev. A **27**, 1389 (1983).
[27]D. J. McLaughlin and Y. Hahn, Phys. Rev. A **28**, 493 (1983).
[28]H. Nussbaumer and P. J. Storey, Astron. Astrophys. **126**, 75 (1983).
[29]A. Pradhan, Phys. Rev. A **30**, 2141 (1984).
[30]S. Geltman, J. Phys. B **18**, 1425 (1985).
[31]G. Alber, J. Cooper, and A. R. P. Rau, Phys. Rev. A **30**, 2845 (1984).
[32]D. C. Griffin, M. S. Pindzola, and C. Bottcher, Phys. Rev. A **31**, 568 (1985).
[33]A. P. Hickman, J. Phys. B **18**, 3219 (1985).
[34]R. L. Brooks, R. U. Datla, and H. R. Griem, Phys. Rev. Lett. **41**, 107 (1978); R. L. Brooks, R. U. Datla, A. D. Krumbein, and H. R. Griem, Phys. Rev. A **21**, 1387 (1980).
[35]C. Breton, C. DeMichelis, M. Finkenthal, and M. Mattioli, Phys. Rev. Lett. **41**, 110 (1978).
[36]R. C. Isler, E. C. Crume, and D. E. Arnurius, Phys. Rev. A **26**, 2105 (1982).
[37]H. C. Meng, H.-J. Kunze, and T. Schmidt, Phys. Lett. **105A**, 221 (1984).
[38]H. C. Meng, P. Greve, H.-J. Kunze, and T. Schmidt, Phys. Rev. A **31**, 3276 (1985).
[39]J. S. Wang, H. R. Griem, R. Hess, W. L. Rowan, and T. P. Kochanski, Phys. Rev. A **33**, 4293 (1986).
[40]M. Bitter, K. W. Hill, M. Zarnstorff, S. von Goeler, R. Hulse, L. C. Johnson, N. R. Sauthoff, S. Sesnic, K. M. Young, M. Tavernier, F. Bely-Dubau, P. Faucher, M. Cornille, and J. Dubau, Phys. Rev. A **32**, 3011 (1985).
[41]M. Bitter, S. von Goeler, S. Cohen, K. W. Hill, S. Sesnic, F. Tenney, and J. Timberlake, Phys. Rev. A **29**, 661 (1984).
[42]F. Bely-Dubau, M. Bitter, J. Dubau, P. Faucher, A. H. Gabriel, K. W. Hill, S. von Goeler, N. Sauthoff, and S. Volante, Phys. Lett. **93A**, 189 (1983).
[43]M. Bitter, S. von Goeler, K. W. Hill, R. Horton, D. Johnson, W. Roney, N. Sauthoff, E. Silver, and W. Stodiek, Phys. Rev. Lett. **47**, 921 (1981).
[44]B. N. Chichkov, M. A. Mazing, A. D. Shevelko, and A. M. Urnov, Phys. Lett. **83A**, 401 (1981).
[45]A. Pospieszczyk, Astron. Astrophys. **39**, 357 (1975).
[46]J. A. Tanis, E. M. Bernstein, W. G. Graham, M. Clark, S. M. Shafroth, B. M. Johnson, K. W. Jones, and M. Meron, Phys. Rev. Lett. **49**, 1325 (1982).
[47]J. A. Tanis, E. M. Bernstein, W. G. Graham, M. P. Stockli, M. Clark, R. H. McFarland, T. J. Morgan, K. H. Berkner, A. S. Schlachter, and J. W. Stearns, Phys. Rev. Lett. **53**, 2551 (1984).
[48]J. A. Tanis, E. M. Bernstein, M. W. Clark, W. G. Graham, R. H. McFarland, T. J. Morgan, B. M. Johnson, K. W. Jones, and M. Meron, Phys. Rev. A **31**, 4040 (1985).
[49]M. Clark, D. Brandt, J. K. Swenson, and S. M. Shafroth, Phys. Rev. Lett. **54**, 544 (1985).
[50]W. A. Schönfeldt, P. H. Mokler, D. H. H. Hoffmann, and A. Warczak, Z. Phys. (to be published).
[51]G. H. Dunn, in *Atomic Processes in Electron-ion and Ion-ion Collisions,* edited by F. Brouillard (Plenum, New York, 1986), p. 93.
[52]D. S. Belić, G. H. Dunn, T. J. Morgan, D. W. Mueller, and C. Timmer, Phys. Rev. Lett. **50**, 339 (1983).
[53]J. B. A. Mitchell, C. T. Ng, J. L. Forand, D. P. Levac, R. E. Mitchell, A. Sen, D. B. Miko, and J. W. McGowan, Phys. Rev. Lett. **50**, 335 (1983).
[54]P. F. Dittner, S. Datz, P. D. Miller, C. D. Moak, P. H. Stelson, C. Bottcher, W. B. Dress, G. D. Alton and N. Nešković, Phys. Rev. Lett. **51**, 31 (1983).
[55]J. F. Williams, Phys. Rev. A **29**, 2936 (1984).
[56]P. F. Dittner, S. Datz, P. D. Miller, P. L. Pepmiller, and C. M. Fou, Phys. Rev. A **33**, 124 (1986).
[57]J. N. Gau and Y. Hahn, J. Quant. Spectrosc. Radiat. Transfer **23**, 121 (1980).
[58]D. C. Griffin and M. S. Pindzola, Phys. Rev. A **35**, 2821 (1987).
[59]K. T. Dolder and B. Peart, Rep. Prog. Phys. **39**, 693 (1976).
[60]A. Müller, N. Djurić, G. H. Dunn, and D. S. Belić, Rev. Sci. Instrum. **57**, 349 (1986).
[61]P. O. Taylor, K. T. Dolder, W. E. Kauppila, and G. H. Dunn, Rev. Sci. Instrum. **45**, 538 (1974).
[62]M. Menzinger and L. Wahlin, Rev. Sci. Instrum. **40**, 102 (1969).
[63]See, for example, J. E. Bayfield, in *The Physics of Electronic and Atomic Collisions,* edited by J. S. Risley and R. Geballe, (University of Washington, Seattle, 1975), p. 727; D. Kleppner, in *Progress in Atomic Spectroscopy,* edited by W. Hanle and H. Kleinpoppen (Plenum, New York, 1979), Part B, p. 713; F. B. Dunning and R. F. Stebbings, Comments At. Mol. Phys. **10**, 9 (1980).
[64]K. B. MacAdam and R. G. Rolfes, Rev. Sci. Instrum. **53**, 592 (1982).
[65]Surface Science Laboratories, Model 2401. This is given for technical completeness only.
[66]H. A. Bethe and E. E. Salpeter, in *Quantum Mechanics of One and Two-Electron Systems,* Vol. 63 of *Handbuch der Physik XXXV, Atoms I,* edited by S. Flügge (Springer-Verlag, Berlin, 1957), pp. 348–355.
[67]R. G. Rolfes, D. B. Smith, and K. B. MacAdam, J. Phys. B **16**, L535 (1983).
[68]D. Richards, J. Phys. B **17**, 1221 (1984).
[69]A. Burgess (private communication).
[70]P. F. Dittner, S. Datz, P. D. Miller, P. L. Pepmiller, and C. M. Fou, Phys. Rev. A **35**, 3668 (1987).
[71]J. L. Kohl, L. D. Gardner, and A. R. Young, Program and Abstracts of the Atomic Physics Program Contractors Workshop, U.S. Department of Energy, held at University of Colorado, April 1986 (unpublished), p. 63.
[72]F. Brouillard, in *Atomic and Molecular Processes in Controlled Thermonuclear Fusion,* edited by C. J. Joachain and D. E. Post (Plenum, New York, 1983).
[73]R. J. Damburg and V. V. Kolosov, J. Phys. B **12**, 2637 (1979).
[74]S. P. Alliluyev and I. A. Malkin, Zh. Eksp. Teor. Fiz. **66**, 1283 (1974). [Sov. Phys.—JETP **39**, 627 (1974).
[75]C. Bottcher (private communication).